Electronic Supplementary Material (ESI) for Journal of Materials Chemistry A.

Solvation Structure Regulation for Ether/Ether Biphasic Electrolyte to Balance Cathodic and Anodic Reactions in Metal-based Battery

Qing Han,[‡a] Shilong Jiao,[‡a] Xiao Liu,[b] Tengfei Bian,[a] Yong Zhao*[a]

[a]Key Lab for Special Functional Materials of Ministry of Education; National & Local Joint Engineering Research Center for High-efficiency Display and Lighting Technology; School of Materials Science and Engineering; Collaborative Innovation Center of Nano Functional Materials and Applications; Henan University, Kaifeng, 475004, P. R. China

[b]College of Chemistry and Chemical Engineering, Henan Key Laboratory of Function-Oriented Porous Materials, Luoyang Normal University, Luoyang, 471934, P. R. China.

‡These authors contributed equally

*Corresponding Author: Y. Zhao (zhaoyong@henu.edu.cn)

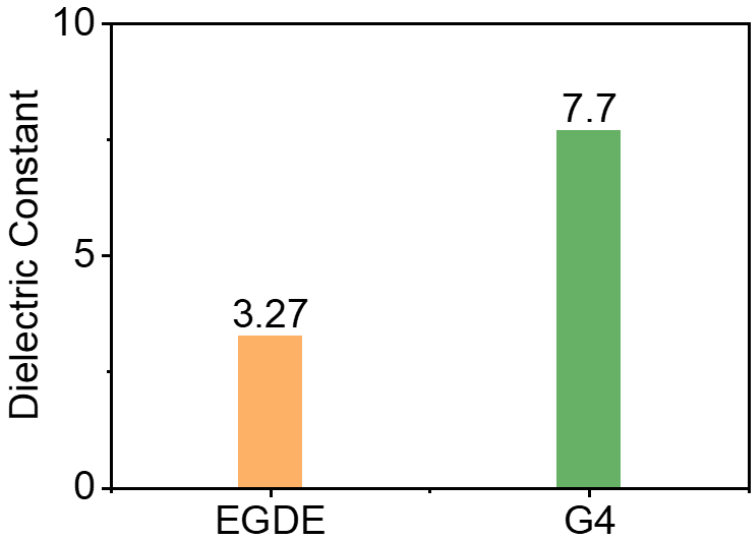

Fig. S1 Dielectric constants of G4 and EGDE solvents.

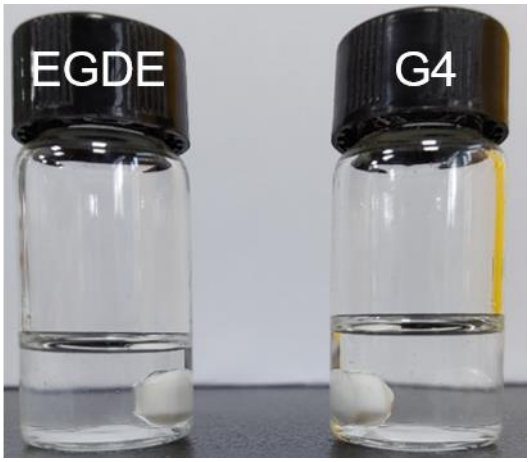

Fig. S2 Optical images of G4 and EGDE based electrolyte with maximum LiTFSI solubility. The concentration of LiTFSI in EGDE is up to 4.0 M (Left), and the concentration of LiTFSI in G4 can reach 6.0 M (Right).

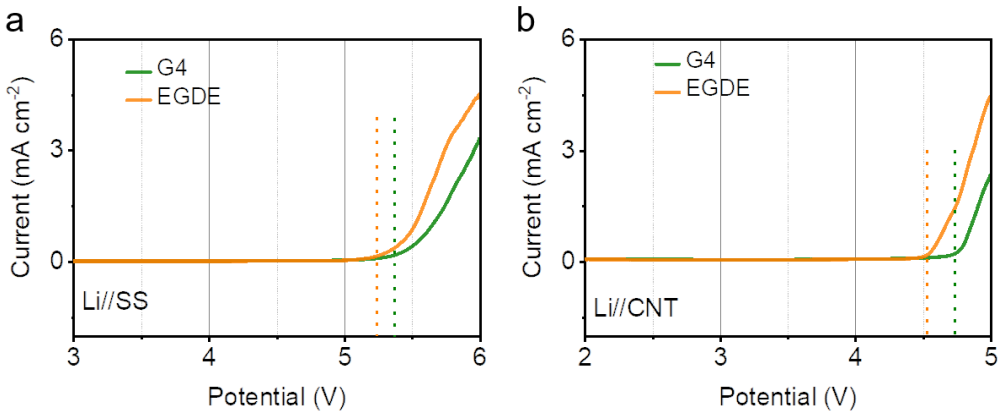

Fig. S3 Linear sweep voltammetry curves of G4 and EGDE solvents with (a) Stainless steel and (b) Carbon nanotubes electrodes.

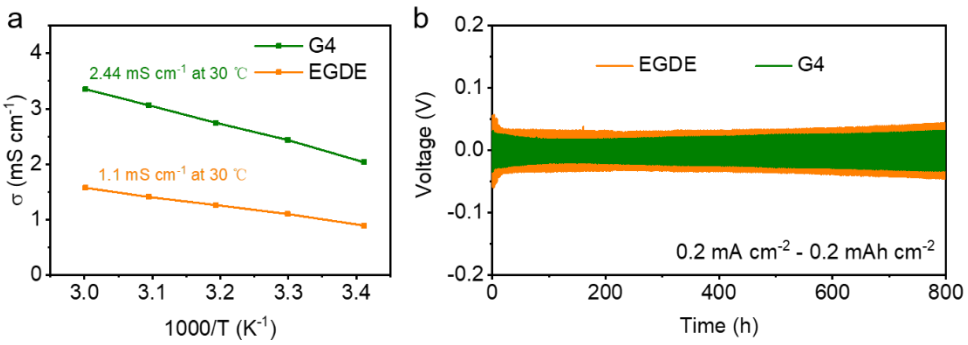

Fig. S4 (a) Temperature-dependent ionic conductivity of G4 and EGDE based electrolytes. (b) The voltage profiles of Li-Li symmetrical cells with G4 and EGDE electrolytes at a current density of 0.2 mA cm^{-2}.

Fig. S5 Optical images of G4 and EGDE mixed solution (G4/EGDE (v/v = 5/5)) with 0.3 M LiTFSI (Left) and 0.4 M LiTFSI (Right).

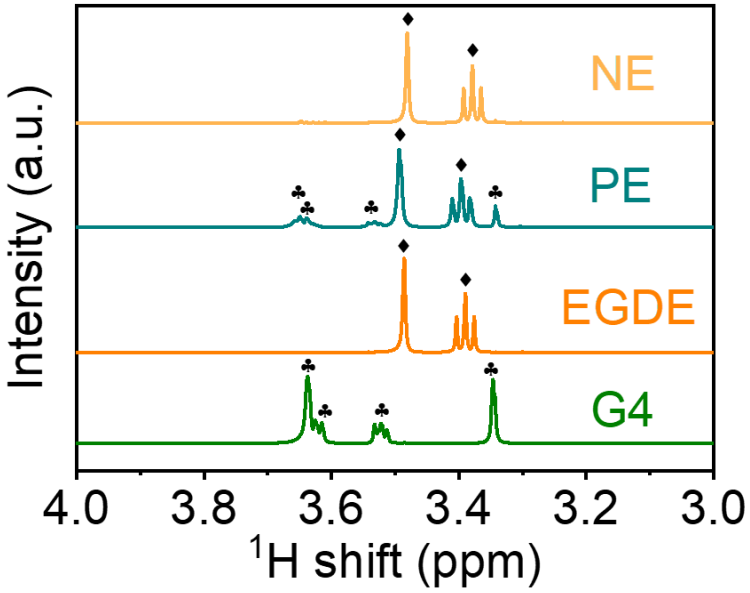

Fig. S6 Enlarged section of the ^{1}H NMR in Fig. 2b.

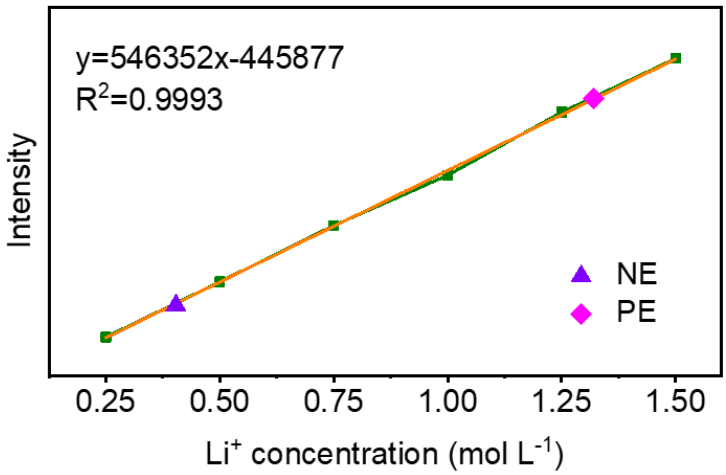

Fig. S7 Quantification of LiTFSI concentrations in ether/ether BLE (1 M LiTFSI in G4/EGDE (v/v = 5/5)) by ICP-AES analysis. LiTFSI concentrations in negative electrolyte (NE) and positive electrolyte (PE).

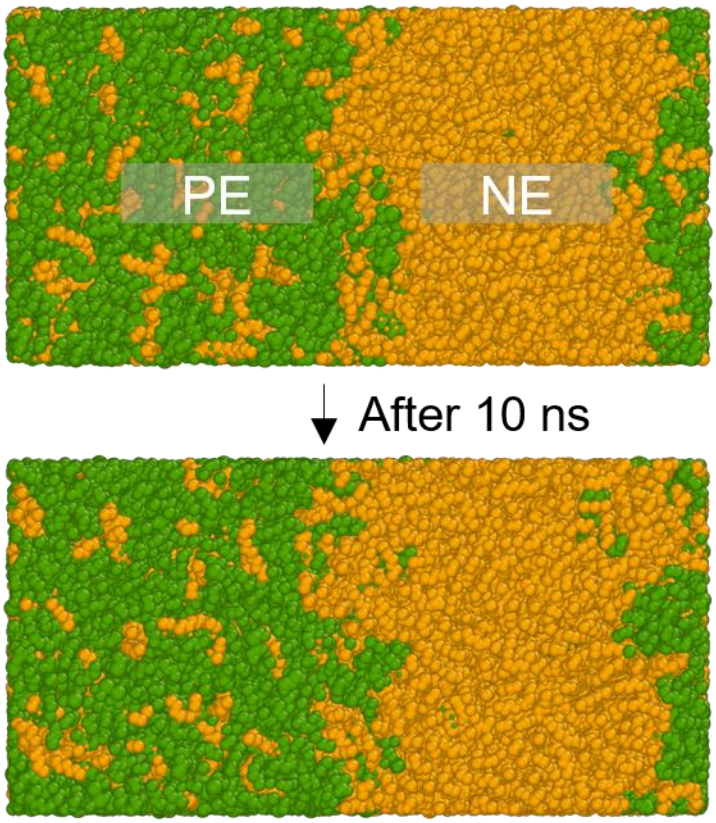

Fig. S8 MD simulations of the immiscible electrolyte mixture in Fig. 2h.

Note: To facilitate the observation of the immiscibility phenomenon of ether/ether BLE, lithium salts were normalized. G4 and EGDE molecules are depicted as green, orange colors, respectively.

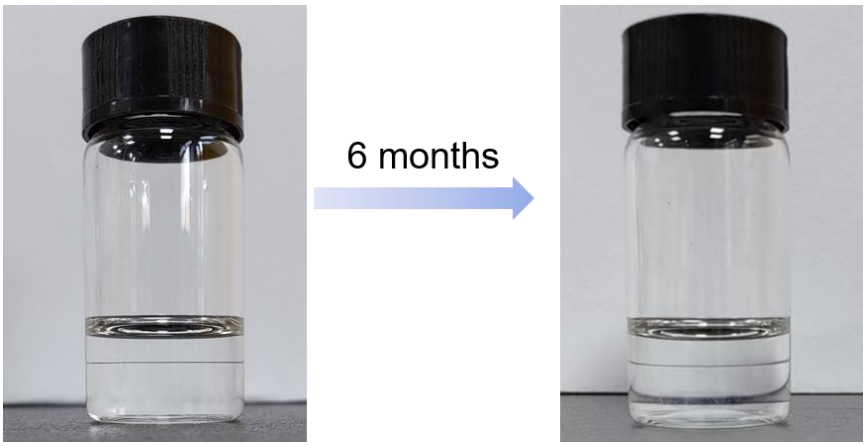

Fig. S9 Optical images of ether/ether based BLEs before and after 6 months.

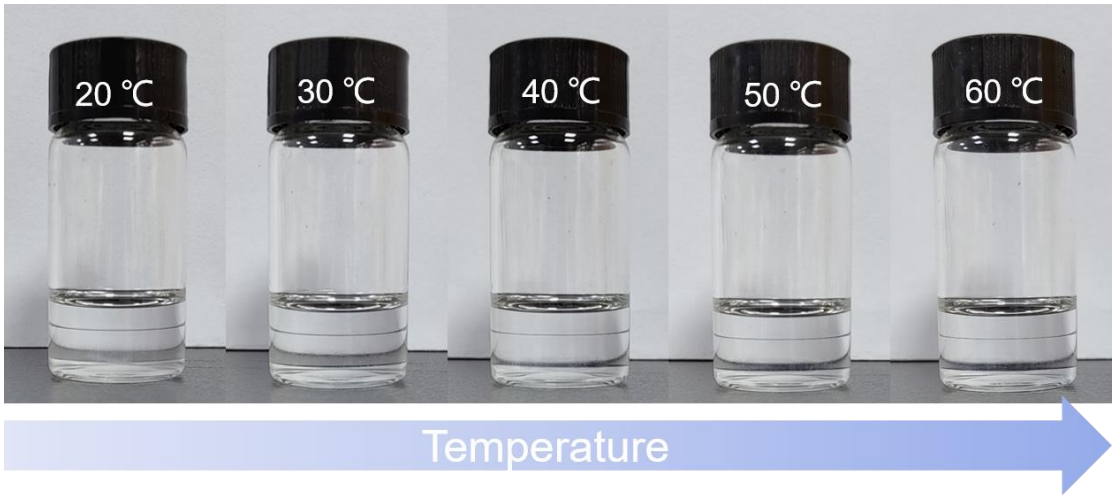

Fig. S10 Optical images of ether/ether based BLEs at different temperatures. As the ambient temperature rises, the electrolyte interface remains clear.

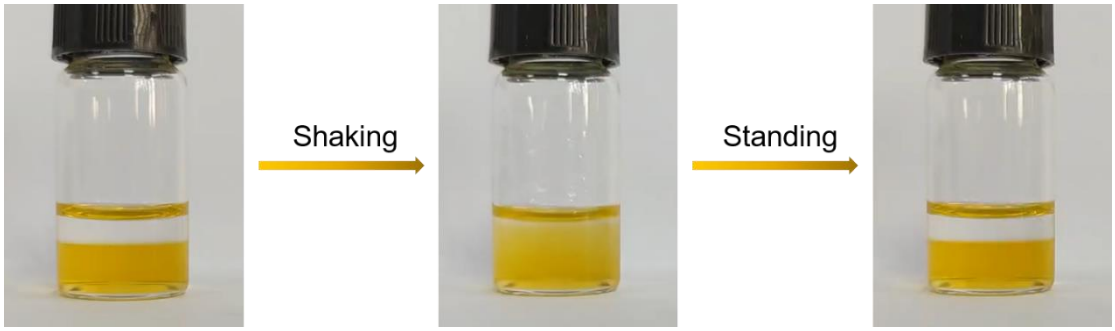

Fig. S11 Optical images of ether/ether based BLE with 20 mM Br_3^- as a color indicator after violent shaking.

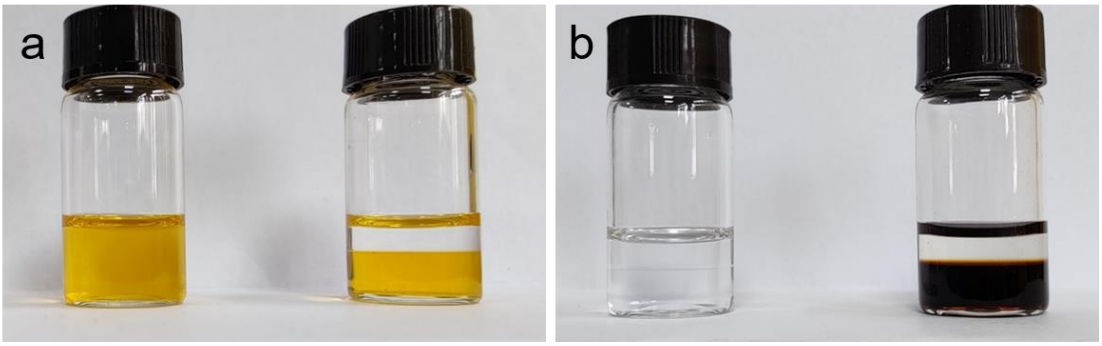

Fig. S12 (a) Photographs of the mixture of 20 mM Br_3^- and solvents (G4/EGDE (v/v = 5/5)) without (left) and with (right) 1 M LiTFSI. (b) Photograph of the mixed electrolyte (1 M LiTFSI in G4/EGDE (v/v = 5/5)) without (left) and with (right) 20 mM LiPSs.

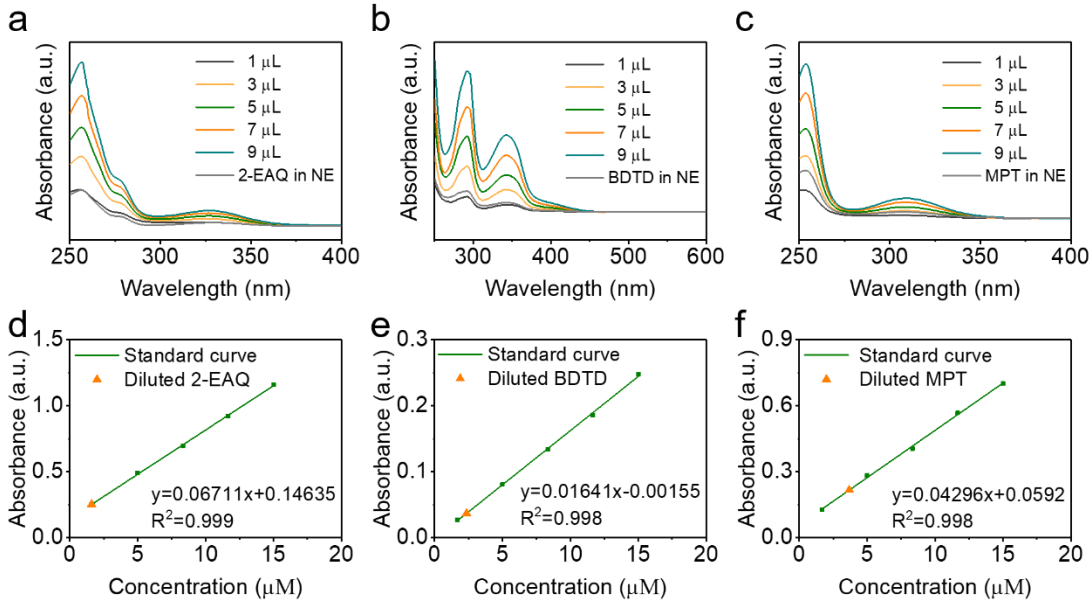

Fig. S13 Quantification of RM concentrations in NE in ether/ether BLE by the UV-Vis absorption spectra. UV-vis absorption spectra of RMs (a, b, c) and the corresponding standard curve and diluted RM concentrations (d, e, f) obtained from the absorption intensity at (a, b, c). (a, d) 2-EAQ. (b, e) BDTD. (c, f) MPT. Note: Quantification of BDTD, 2-EAQ, MPT concentrations in NE: BDTD, 2-EAQ, MPT (5 mM) were dissolved in G4 (1 mL), and then 1 uL, 3 uL, 5 uL, 7 uL, 9 uL of above samples were dispersed in G4 (3 mL) and UV-Vis absorption spectra were recorded. The standard curves are obtained from the linear relation between BDTD, 2-EAQ and MPT concentrations and absorbance intensity. Subsequently, 10 uL of NE (20 mM RM) was added into 3 mL G4 solvent to obtain the diluted RM solution, and the corresponding absorption intensity was recorded. Finally, the diluted BDTD, 2-EAQ, and MPT concentrations calculated from the absorption intensities were 2.349, 1.589, and 3.673 μM, respectively. It can be seen that the concentrations of BDTD, 2-EAQ and MPT before dilution are 0.7, 0.48 and 1.1 mM, respectively.

Fig. S14 The structure of beaker cells with the SLE (1 M LiTFSI in G4, left) and BLE (1 M LiTFSI in G4/EGDE (v/v = 5/5), right). Lithium foil and CNTs were used as the negative and positive electrode, respectively.

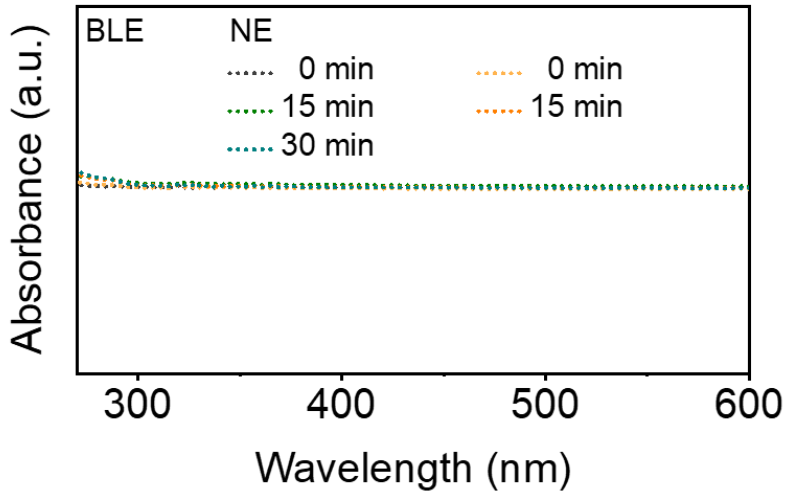

Fig. S15 Enlarged section of the UV-vis absorption spectra curves of Br_3^- in NE in Fig. 4c.

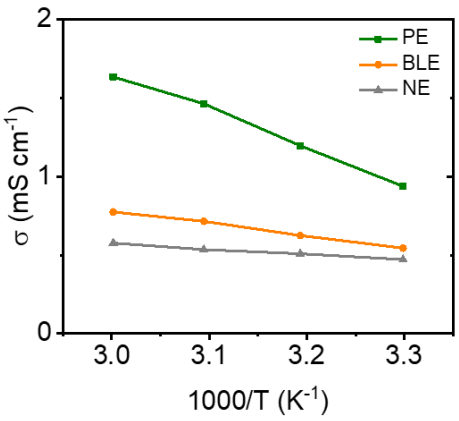

Fig. S16 Temperature-dependent ionic conductivity of the PE, NE and BLE.

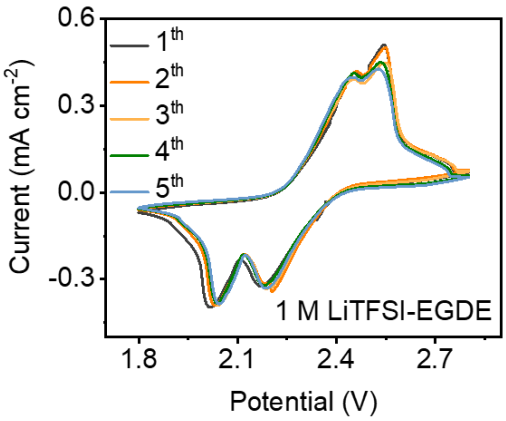

Fig. S17 CV curves of 0.2 M 2-EAQ in EGDE (1 M LiTFSI) electrolyte in the voltage range between 1.8 V and 2.8 V.

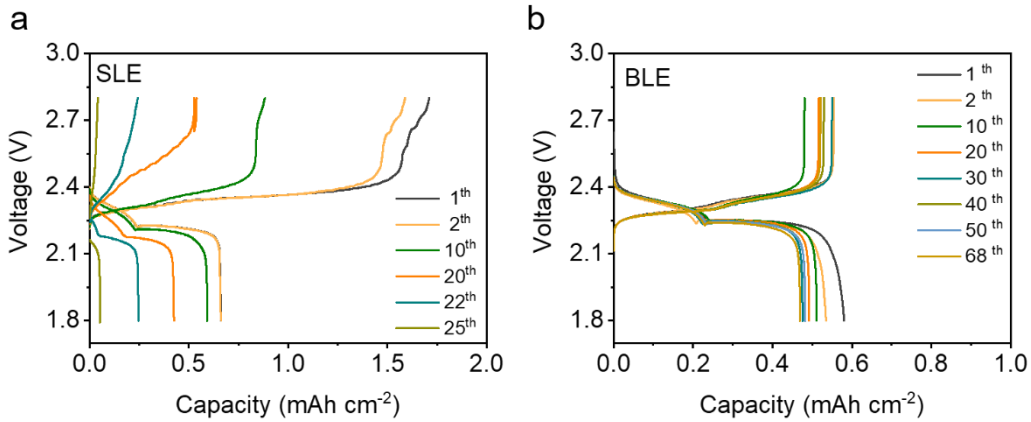

Fig. S18 Cell voltage profiles versus capacities in (a) SLE and (b) BLE at various cycle numbers.

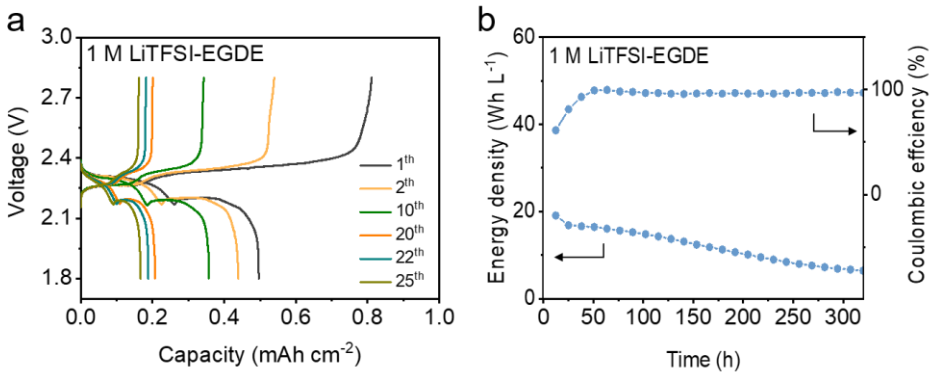

Fig. S19 (a) Cell voltage profiles versus capacities in EGDE (1 M LiTFSI) electrolyte at various cycle numbers. (b) Coulombic efficiency and specific discharge energy densities as a function of cycle time (the specific energy density is calculated according to the electrolyte volume) in static LRFBs with EGDE (1 M LiTFSI) electrolyte.

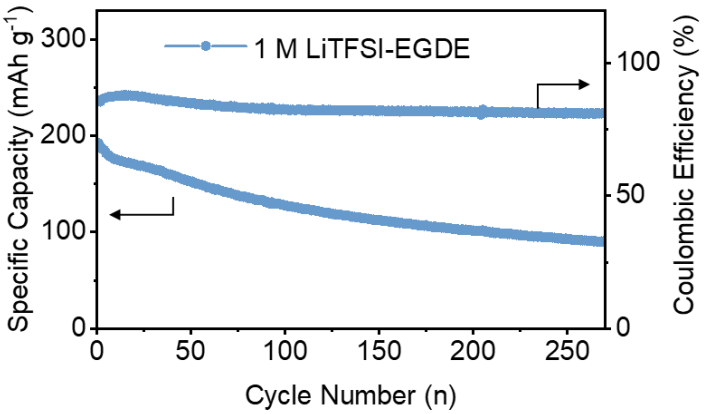

Fig. S20 Cycling performances of static Li-SFBs with EGDE (1 M LiTFSI) electrolyte.

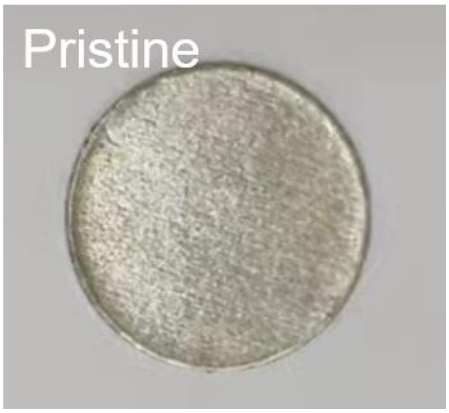

Fig. S21 Photograph of lithium anode before cycle.

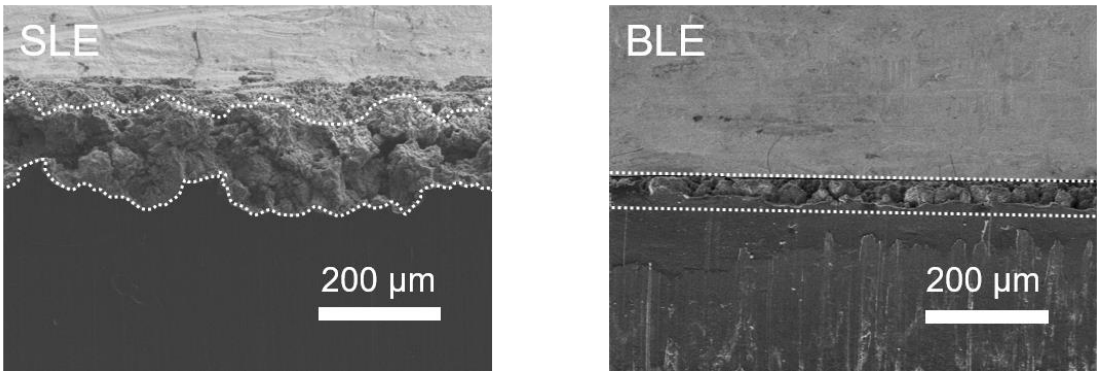

Fig. S22 Front view of SEM images of Li metal with 10 cycles using SLE or BLE.

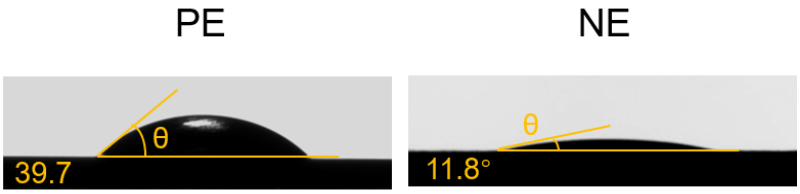

Fig. S23 Contact angle measurement of PE and NE on the lithium foil surface.

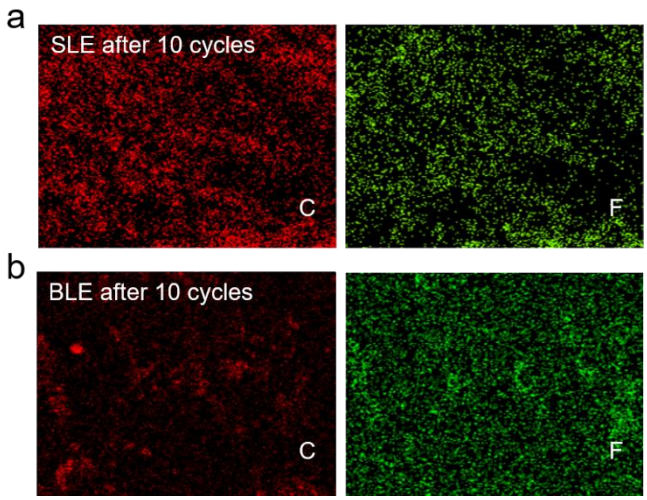

Fig. S24 Energy-dispersive X-ray spectroscopy (EDS) elemental mapping of the Li anodes after 10 cycles in Li-O_2 batteries with SLE or BLE.

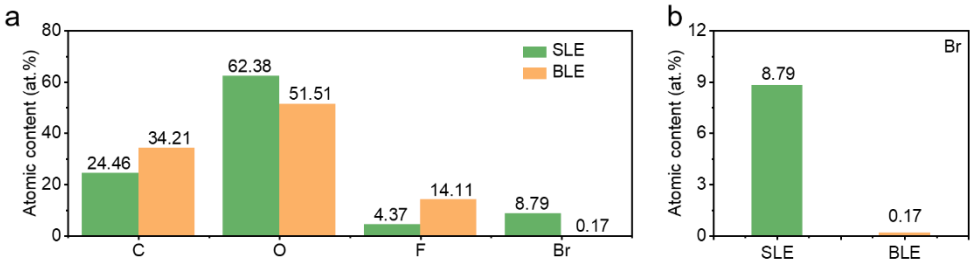

Fig. S25 (a) Surface element content of Li anode in Li-O_2 cells with SLE or BLE after 10 cycles. (b) Enlarged section of the Br element content in (a).

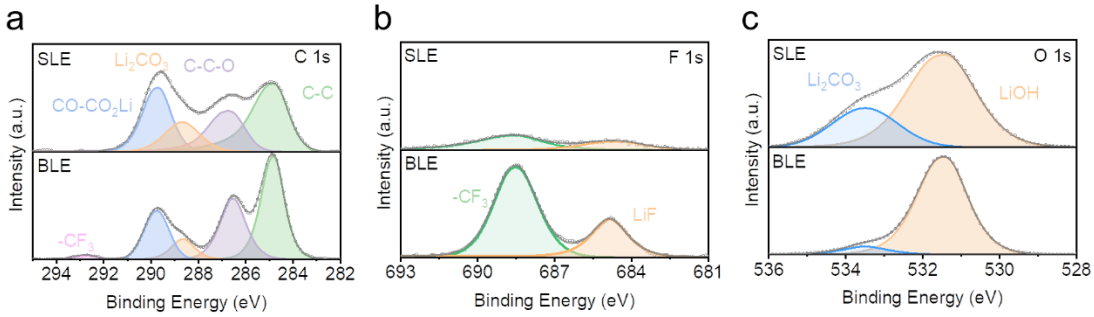

Fig. S26 XPS spectra of C 1s, F 1s, and O 1s for the surface of Li anode in the Li-O_2 cells with SLE and BLE after 10 cycles. (a) C 1s. (b) F 1s. (c) O 1s.

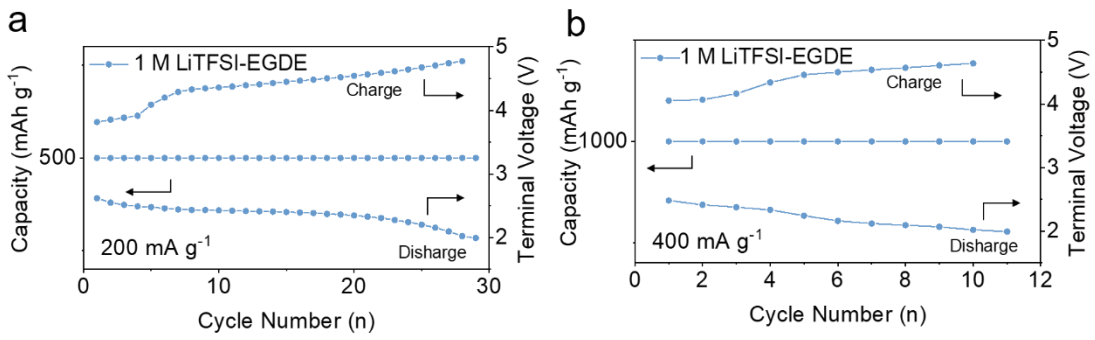

Fig. S27 Cycling performance of Li-O_2 cells with EGDE (1 M LiTFSI) electrolyte at a current density of 200 mA g^{-1} with a fixed capacity of 500 mAh g^{-1} (a), and at a current density of 400 mA g^{-1} with a fixed capacity of 1000 mAh g^{-1} (b).